Journal of Reproduction and Development, Vol. 60, No 6, 2014

—Technology Report—

Correlations among antral follicular echotexture, apoptosis and expression of key steroidogenic enzymes in sheep

Taylor VANDUZER[1)], Raj DUGGAVATHI[2)], Maciej MURAWSKI[3)], Dorota A. ZIEBA[3)], Patrycja SROKA[3)] and Pawel M. BARTLEWSKI[1)]

[1)]*Department of Biomedical Sciences, Ontario Veterinary College, University of Guelph, Guelph ON, N1G 2W1 Canada*
[2)]*Department of Animal Science, McGill University, Ste-Anne-de-Bellevue QC, H9X 3V9 Canada*
[3)]*Department of Swine and Small Ruminant Breeding, University of Agriculture in Kraków, 30-274 Kraków, Poland*

Abstract. Nineteen cycling ewes underwent transrectal ultrasonography of ovaries followed by ovariectomies during the growth phase of the first follicular wave of the interovulatory interval or the proestrus/estrus phase of the cycle. Quantitative ultrasonographic characteristics of the antrum and follicular wall in a total of forty-three ovine antral follicles were examined for correlations with the protein expression of three steroidogenic enzymes (cytochrome P450 17α-hydroxylase, CYP17; cytochrome P450 aromatase, CYP19; and 3β-hydroxysteroid dehydrogenase, 3β-HSD) determined by densitometric analysis of immunohistochemical slides, follicular dimensions, granulosa layer thickness and the percentage of apoptotic granulosa cells. Significant correlations were found between echotextural attributes of ovine antral follicles and the percentage of apoptotic granulosa cells, CYP17 expression (theca), CYP19 expression (granulosa) and 3β-HSD expression (theca cells). Computer-aided analyses of ultrasonographic images can be beneficial to the development of assisted reproductive technologies and diagnosis of hormonal imbalances without the need for ovarian biopsies or hormone assays.

Key words: Computerized image analysis, Histomorphology, Ovarian antral follicles, Sheep, Steroidogenic enzymes, Ultrasonography

(**J. Reprod. Dev. 60:** 476–482, 2014)

Determining the expression of steroidogenic enzymes in ovarian follicles is an important diagnostic and research tool. Abnormalities in the activity of steroidogenic enzymes can be associated with a vast array of pathophysiological conditions including, but not limited to, infertility, virilization, abnormal sexual development, polycystic ovary syndrome, osteoporosis and pseudohermaphroditism [1–3]. Quantifying steroidogenic enzyme proteins *in situ* would allow us to identify and "locate" the reasons for abnormal hormone levels. In animals and humans undergoing ovarian stimulation procedures, rapid and noninvasive estimation of steroidogenic enzyme expression at the level of individual antral follicles would facilitate the selection of follicles for oocyte aspiration [4].

The expression patterns of key steroidogenic enzymes of the estrogen production pathway have previously been studied at different stages of the ewe's ovulatory cycle mainly by ovariectomies [5–7]. Ultrasonographic imaging is the key to performing ovarian assessments without the use of invasive procedures [8]. Diagnostic ultrasonography utilizes high-frequency sound waves that interact at tissue boundaries and interfaces. Gray-scale diagnostic ultrasonography combined with computer-assisted analysis of ultrasonograms enables evaluation of the physiological status of individual ovarian structures with a single examination of the whole ovary [9, 10]. The ultrasonographic appearance of a tissue is referred to as the echotexture. Quantitative echotextural variables are the measures of pixel intensity and uniformity within an ultrasonogram. The use of computer-assisted analysis of ultrasonographic images has made it possible to determine objectively the echotextural variables (i.e., numerical pixel values and heterogeneity) within discrete regions of individual antral follicles [8–10]. In bovine and ovine ovarian antral follicles, these variables have been found to correlate with circulating or follicular fluid levels of estrogens [5, 10, 11]. Increased steroidogenesis during antral follicular lifespan is caused by an increase in protein expression of steroidogenic enzymes in healthy, non-atretic antral follicles [5], and the changes in protein content of gonadal tissues are associated with the changes in their echotexture [12].

Therefore, we hypothesized that antral follicular echotexture would be indicative of the protein expression of key steroidogenic enzymes at various stages of follicular growth and secretory activity. We determined the echotextural parameters and expression of three steroidogenic enzymes, namely cytochrome P450 17α-hydroxylase (CYP17), cytochrome P450 aromatase (CYP19) and 3β-hydroxysteroid dehydrogenase (3β-HSD), in small, medium and large ovine antral follicles of the first follicular wave of the estrous cycle, and in preovulatory follicles. We also examined follicular ultrasonographic characteristics for correlations with histological (granulosa layer thickness) and functional attributes (apoptotic rate of granulosa cells). Pairing ovarian ultrasonography with computer-assisted

Received: May 21, 2014
Accepted: July 6, 2014
Published online in J-STAGE: August 11, 2014

Correspondence: M Murawski (e-mail: rzmuraw@cyf-kr.edu.pl)

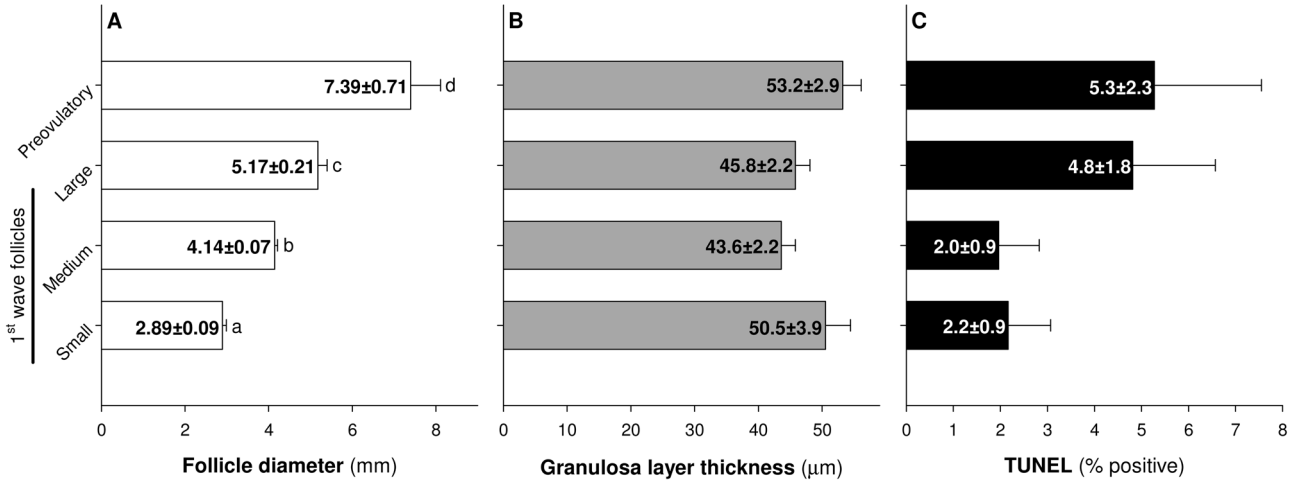

Fig. 1. Follicle diameters (A), granulosa layer thickness (B) and percentages of TUNEL-positive granulosa cells (C) (mean ± SEM) for small (≥2.00 mm and ≤ 3.50 mm, n = 18), medium (> 3.50 mm and ≤ 4.50 mm, n = 9) and large (> 4.50 mm in diameter, n = 11) follicles of the first follicular wave of the interovulatory interval studied, and preovulatory follicles (n = 5) detected ultrasonographically and dissected from 19 cycling Western White Face ewes. a–d: mean values denoted by different letters vary significantly (P<0.05).

image analysis could remove the need for ovariectomies or ovarian biopsies and hence greatly diminish the pain and stress as well as the extensive labor and cost currently associated with ovarian assessment. This noninvasive technique would expand the use of ovarian assessment onto women by bypassing many ethical issues previously associated with invasive procedures, and it can be easily and frequently repeated. It would also provide more rapid results than the hormonal assays presently used.

The mean diameters of the growing antral follicles of the first wave of the estrous cycle and of the preovulatory follicles (measurements taken from recorded images using the Image-Pro Plus® analytical software) are shown in Fig. 1A. There were no significant differences in the granulosa layer thickness (Fig. 1B) and proportions of apoptotic cells detected by TUNEL (terminal deoxynucleotidyl transferase-mediated dUTP-biotin nick end labeling; Fig. 1C) among the follicle categories.

The specific absorptive indices (enzyme expression) for CYP17 (theca) and 3β-HSD (theca) recorded in the immunohistochemically stained slides were greater ($P < 0.05$) in large ovarian follicles compared with small ovarian follicles, whereas the expression of CYP19 (granulosa) was greater ($P < 0.05$) in both the medium-sized and large antral follicles than in small follicles of the first wave of the interovulatory interval (Fig. 2). The expression of 3β-HSD was greater ($P < 0.05$) in the granulosa cells from preovulatory ovine follicles compared with that in the granulosa cells from small follicles of the first follicular wave (Fig. 2).

There were numerical but not significant differences in the echotextural parameters determined by spot analysis of the follicle antrum (Table 1) and line analysis of the three segments encapsulating the follicle wall (Table 2) among the four follicle categories.

The specific absorptive indices for CYP17 correlated with the mean numerical pixel values (NPVs; $r = 0.46$, $P = 0.01$), pixel heterogeneity ($r = 0.51$, $P = 0.004$), and minimum ($r = 0.48$, $P = 0.008$) and maximum ($r = 0.39$, $P = 0.03$) gray-scale values determined by spot analysis of the follicular antrum (Table 3). The expression of CYP17 also correlated with the slope value for segments 1 and 2 (the peripheral antrum and follicle wall proper, respectively; both $r = 0.36$, $P = 0.05$) as well as the *y*-intercept of segment 2 ($r = 0.36$, $P = 0.05$). The expression of CYP19 correlated with the mean pixel intensities of segment 1 ($r = 0.36$, $P = 0.04$) as well as the slope value for segments 1 and 2, and the *y*-intercept of segment 2 (all $r = 0.37$, $P < 0.05$; Table 3). The protein expression of 3β-HSD (theca) correlated with the mean NPVs within the spot ($r = 0.43$ $P = 0.05$; Table 3). The percentage of apoptotic cells determined by TUNEL correlated directly with the follicle diameter ($r = 0.45$, $P = 0.01$) and inversely with the minimum grey scale value of the spot ($r = -0.43$, $P = 0.02$; Table 3). The percentage of TUNEL-positive granulosa cells correlated with the slope value for segment 1 ($r = -0.38$, $P = 0.04$); mean pixel intensity ($r = -0.39$, $P = 0.03$), slope ($r = -0.38$, $P = 0.04$) and *y*-intercept ($r = -0.37$, $P = 0.05$) of segment 2; and the pixel heterogeneity ($r = 0.63$, $P = 0.0003$), slope value ($r = 0.63$, $P < 0.0003$) and *y*-intercept ($r = -0.37$, $P = 0.05$) of segment 3 (perifollicular stroma).

A systematic study analyzing the direct temporal relationships between echotextural variables and histomorphological attributes of ovine antral follicles has not yet been reported. This study is also the first to look at whether correlations exist between the expression of steroidogenic enzymes (CYP17, CYP19 and 3β-HSD) and echotextural attributes of ovarian antral follicles at various stages of growth and different stages of the estrous cycle.

Using spot analyses of the follicular antrum, it was found that there was no significant difference in quantitative echotextural variables between any of the follicle categories. The results of line analyses did not reveal any differences in follicular wall echotexture among various types of ovine antral follicles studied. These findings are in disagreement with earlier bovine studies. For example, in cattle,

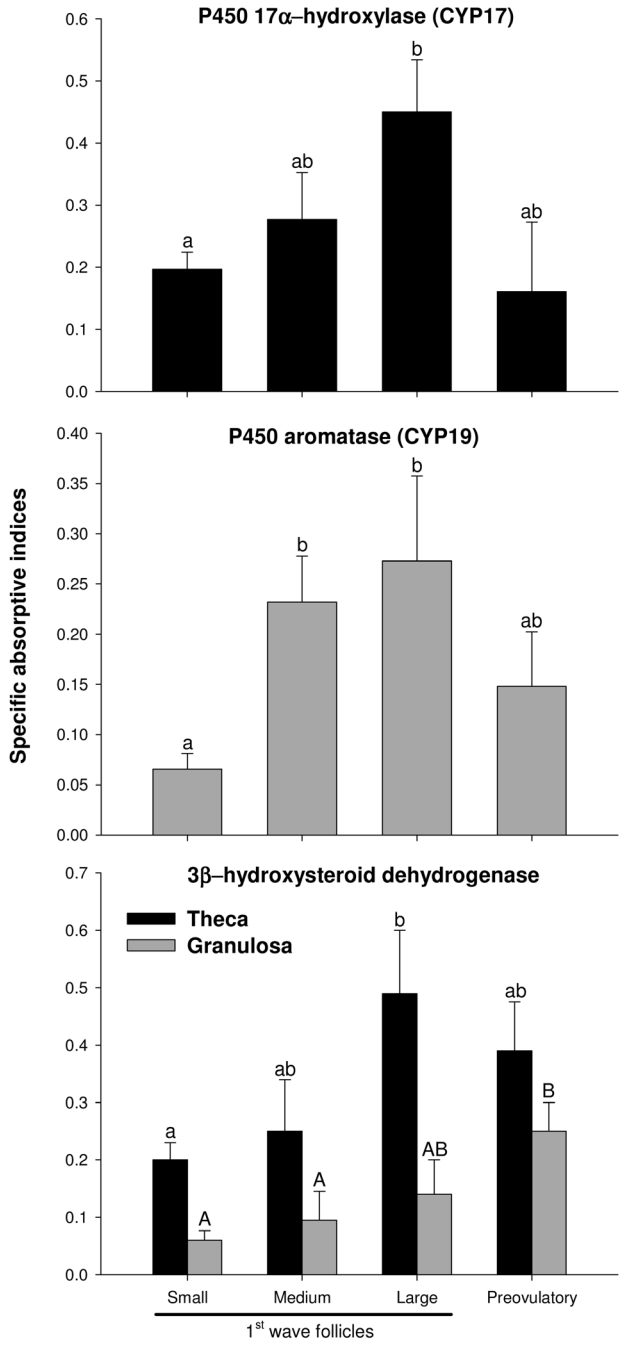

Fig. 2. Variance in the expression of 17α-hydroxylase (CYP17), aromatase (CYP19) and 3β-hydroxysteroid dehydrogenase in small (≥ 2.00 mm and ≤ 3.50 mm, n = 18), medium (> 3.50 mm and ≤ 4.50 mm, n = 9) and large (> 4.50 mm in diameter, n = 11) follicles of the first follicular wave of the interovulatory interval studied, and preovulatory follicles (n = 5) collected from 19 cyclic Western White Face ewes and determined by gray-scale densitometric analysis of immunohistochemical slides. For each enzyme, means denoted by different letters (ab, AB) differ ($P<0.05$).

there was a significant difference in mean pixel values and pixel heterogeneity of the antrum between the preovulatory stage compared with an early stage of the dominant follicle lifespan (first wave of the estrous cycle [10, 14]), and the mean pixel values for the follicle wall proper and perifollicular stroma increased during the growth phase of the dominant follicle (wave I) and were lowest in the preovulatory follicles [10]. Singh *et al*. [10] suggested that the changes in the follicular echotexture were due to a decrease in the thickness of the granulosa layer caused by the sloughing of apoptotic granulosa cells [10]. A study by Liu *et al*. [9] also recorded a negative correlation between follicular diameter and granulosa layer thickness for bovine ovaries *ex situ*. In the present experiment, however, there was no variance in the granulosa layer thickness and no significant shift in the level of granulosa cell apoptosis among different size classes or stages of follicular development. Moreover, quantitative echotextural variables were not correlated with granulosa layer thickness in ewes, but associations were seen among the ultrasonographic image characteristics, immunohistochemical enzyme expression levels and estimates of granulosa cell apoptosis.

CYP17 is responsible for the conversion of pregnenolone to 17α-hydroxypregnenolone and subsequently dehydroepiandrosterone [15]. It is a key enzyme in the biosynthesis of progestins, glucocorticoids, androgens, estrogens and mineralocorticoids. CYP19 is a key steroidogenic enzyme in the synthesis of estrogens from androgens [13], whereas 3β-HSD is essential to catalyze numerous reactions in the steroidogenic pathway [16]. In the present study, CYP17 expression directly correlated with mean numerical pixel values, pixel heterogeneity, and minimum and maximum gray-scale values determined by spot analysis of the follicular antrum. The reason for a lack of similar correlations for CYP19 (expressed in follicular granulosa cells) and 3β-HSD (located in both the theca and granulosa layers) is unknown. In this study, there was also a positive correlation between the protein expression of CYP17 and echotextural characteristics of segments 1 and 2 (the slope of segment 1 and the slope and intercept of segment 2). This is consistent with the findings of a linear relationship between circulating estradiol concentrations and echotextural characteristics of the follicular wall recorded in preovulatory ovine follicles [11]. The existence of correlations between CYP17 and segment 1 was unexpected because this segment includes mainly the edge of the antrum and granulosa layer, and CYP17 is only expressed in theca cells [7]. The presence of these correlations may indicate that segment 1 actually did reach into the theca layer. Line analysis of the area encompassing the follicle wall included three segments to represent morphologically distinct regions of the follicle comprising mainly, but not exclusively, the peripheral antrum, follicle wall proper and perifollicular ovarian stroma. If segment 1 extended all the way into the theca layer and the beginning of segment 2 also included theca cells, this would explain the correlations between the expression of CYP17 and quantitative echotextural variables of both segments.

Significant positive correlations were found between the protein abundance of CYP19 and mean pixel intensities and slope of segment 1, and between the protein abundance of CYP19 and the slope and intercept values for segment 2. These correlations are consistent with the finding that CYP19 is detected in the granulosa layer of growing antral follicles [7], as the segment 1 and 2 pixel lengths may both

Table 1. Quantitative echotextural variables (mean ± SEM) determined by spot analysis of the follicular antrum using Image ProPlus® analytical software

Echotextural variables	Follicle category			
	1st wave follicles			Preovulatory (n = 5)
	Small (n = 18)	Medium (n = 9)	Large (n = 11)	
NPVs	29.1 ± 2.3	28.1 ± 2.1	28.7 ± 3.6	20.1 ± 0.7
SD	6.6 ± 0.4	6.5 ± 0.7	7.1 ± 1.0	4.3 ± 0.8
MIN	15.1 ± 1.5	13.4 ± 0.6	13.5 ± 1.9	9.0 ± 1.1
MAX	49.3 ± 3.0	50.8 ± 4.3	56.6 ± 5.4	43.8 ± 5.0

Computerized image analyses were performed on 43 ultrasonograms obtained in 19 cycling Western White Face ewes during the period encompassing the growth phase of the first follicular wave of the ovulatory cycle and the ensuing proestrus/estrus phase (preovulatory follicles). NPVs, numerical pixels values or pixel intensity; SD, standard deviation of mean numerical pixel values or pixel heterogeneity; MIN, minimum pixel value within a spot meter; and MAX, maximum pixel value within a spot meter.

Table 2. A summary of echotextural variables (mean ± SEM) determined by line analysis of the region straddling the follicular wall (three pixel segments: 1–3) using Image ProPlus® analytical software

Echotextural variables	Follicle category	Line segment		
		Segment 1 (peripheral antrum)	Segment 2 (follicular wall proper)	Segment 3 (perifollicular stroma)
NPVs	1st wave-Small	38.2 ± 1.5	51.1 ± 1.6	63.2 ± 1.6
	1st wave-Medium	37.3 ± 2.3	51.1 ± 2.8	63.5 ± 3.2
	1st wave-Large	36.6 ± 2.4	49.2 ± 2.2	63.6 ± 2.5
	Preovulatory	33.3 ± 2.7	45.1 ± 2.6	57.7 ± 2.5
SD	1st wave-Small	5.3 ± 0.5	7.6 ± 0.6	4.6 ± 0.5
	1st wave-Medium	8.7 ± 3.0	7.8 ± 1.0	4.6 ± 0.4
	1st wave-Large	4.4 ± 0.5	8.1 ± 0.6	6.3 ± 0.8
	Preovulatory	4.8 ± 0.9	6.7 ± 0.3	5.8 ± 0.7
Slope	1st wave-Small	9.5 ± 1.0	13.1 ± 1.1	8.1 ± 0.9
	1st wave-Medium	10.5 ± 1.6	14.1 ± 1.8	8.4 ± 0.9
	1st wave-Large	7.9 ± 0.9	14.5 ± 1.2	11.3 ± 1.4
	Preovulatory	8.7 ± 1.6	12.0 ± 0.6	10.4 ± 1.2
Intercept	1st wave-Small	33.2 ± 1.6	43.5 ± 1.7	58.7 ± 1.7
	1st wave-Medium	31.4 ± 2.3	43.2 ± 2.6	58.9 ± 3.2
	1st wave-Large	32.1 ± 2.7	41.0 ± 2.1	57.3 ± 2.4
	Preovulatory	28.8 ± 2.9	38.4 ± 2.8	51.9 ± 2.4

Computerized analyses were performed on 43 ovarian ultrasonographic images obtained in 19 cycling Western White Face ewes during the period encompassing the growth phase of the first follicular wave of the ovulatory cycle (small (n = 18), medium (n = 9) and large (n = 11) antral follicles) and preovulatory follicles (n = 5) detected during the ensuing proestrus/estrus phase. NPVs, numerical pixels values or pixel intensity; SD, standard deviation of numerical pixel values or pixel heterogeneity.

have included the granulosa layer, while the slope of each region is an indicator of the relative change in the gray-scale value of successive pixels from the beginning to the end of a given segment [10]. The expression of 3β-HSD in theca cells was significantly correlated with the mean gray-scale values within the antrum. Immunohistochemical detection of 3β-HSD, the only enzyme analyzed in the present study expressed in both the theca and granulosa cells, was not associated with echotextural variables determined by line analysis.

The results of TUNEL (% of apoptotic granulosa cells) significantly correlated with follicle size, indicating that as the follicle grows, the rate of atresia increases. This correlation, however, appears to be due mainly to an increase in the rate of granulosa cell apoptosis between small/medium and large/preovulatory ovarian follicle stages (Fig. 1). There was also a significant correlation between TUNEL results and the minimum gray-scale value obtained by spot analysis, suggesting that the rate of apoptosis and pixel intensity of the follicular antrum increase in parallel. Finally, there were significant correlations between TUNEL results and echotextural parameters of all three pixel segments used for the line analysis. Consequently, computer-assisted analyses of ovarian ultrasonographic images *in situ* holds promise to become a highly beneficial method in the diagnosis of ovarian hormonal imbalances caused by variations

Table 3. Correlations among follicular diameter, echotextural variables of the follicular antrum (spot analysis) and wall (line analysis), steroidogenic enzyme protein abundance and TUNEL results (% of apoptotic granulosa cells) determined for ovarian follicles (n = 43) from 19 cycling Western White Face ewes

Variables	CYP17 (theca)	CYP19 (granulosa)	3β-HSD (theca)	3β-HSD (granulosa)	TUNEL
Follicle diameter	NS	NS	NS	NS	r = 0.45, P = 0.01
Spot NPVs	r = 0.46, P = 0.01	NS	r = 0.43, P = 0.05	NS	NS
Spot SD	r = 0.51, P = 0.004	NS	NS	NS	NS
Spot MIN	r = 0.48, P = 0.008	NS	NS	NS	r = −0.43, P = 0.02
Spot MAX	r = 0.39, P = 0.03	NS	NS	NS	NS
Segment 1 NPVs	NS	r = 0.36, P = 0.04	NS	NS	NS
Segment 1 SD	NS	NS	NS	NS	NS
Segment 1 slope	r = 0.36, P = 0.05	r = 0.37, P = 0.03	NS	NS	r = −0.38, P = 0.04
Segment 1 intercept	NS	NS	NS	NS	NS
Segment 2 NPVs	NS	NS	NS	NS	r = −0.39, P = 0.03
Segment 2 SD	NS	NS	NS	NS	NS
Segment 2 slope	r = 0.36, P = 0.05	r = 0.37, P = 0.03	NS	NS	r = −0.38, P = 0.04
Segment 2 intercept	r = 0.36, P = 0.05	r = 0.37, P = 0.03	NS	NS	r = −0.37, P = 0.05
Segment 3 NPVs	NS	NS	NS	NS	NS
Segment 3 SD	NS	NS	NS	NS	r = 0.63, P = 0.0003
Segment 3 slope	NS	NS	NS	NS	r = 0.63, P = 0.0003
Segment 3 intercept	NS	NS	NS	NS	r = −0.37, P = 0.05

NPVs, numerical pixels values or pixel intensity; SD, standard deviation of numerical pixel values or pixel heterogeneity; MIN, minimum pixel value within a spot meter; MAX, maximum pixel value within a spot meter; r, coefficient of correlation; CYP17, 17α-hydroxylase; CYP19, aromatase; 3β-HSD, 3β-hydroxysteroid dehydrogenase; TUNEL, terminal deoxynucleotidyl transferase-mediated dUTP-biotin nick end labeling.

in steroidogenic enzyme expression and the development of new assisted reproductive technologies.

Methods

Ovine ovaries and ultrasonographic imaging

The present study used retrospective analyses of the data originally collected by Duggavathi *et al.* [7] but with a more discriminating classification of ovarian antral follicles and new statistical analyses of the echotextural and histophysiological ovarian data (Pearson's product-moment or correlation analyses). Transrectal ovarian ultrasonography was performed on cycling Western White Face ewes (October-November) twice a day beginning at the onset of behavioral estrus (nonsynchronized, spontaneously occurring estrous cycles) detected with vasectomized crayon-harnessed rams. All examinations were performed by one experienced operator. Animals were housed in sheltered dry lots at the University of Saskatchewan (Saskatoon, Saskatchewan, Canada; *latitude* 52°10'N and *longitude* 106°41'W) and received daily maintenance feed rations with alfalfa hay, water and mineralized salt licks available *ad libitum*.

Ultrasonography utilized a real-time B-mode echo camera (Aloka SSD-900; Aloka, Tokyo, Japan) connected to a stiffened 7.5-MHz linear-array transducer. Images were displayed at an image magnification of 2.5 × and were recorded on high-grade video tapes (Fuji S-VHS, ST-120 N) for analysis of ovarian data at a later date. Antral follicles were initially measured to the nearest 1 mm using internal electronic calipers. Mean follicular diameters (average of two dimensions, vertical and horizontal) were taken from the still images. Selected still images were digitized at standardized settings, at a resolution of 720 × 480 pixels and with 256 shades of gray using digital image-acquisition software (Adobe Premiere®Pro 1.5, Adobe Systems, San Jose, CA, USA) and stored as graphic images.

The ewes were randomly divided into 4 groups and ovariectomized [7] when the largest follicle(s) of the first wave of the estrous cycle reached a diameter of 3 mm (n = 4), 4 mm (n = 5) or ≥ 5 mm (n = 5). In the fourth group (n = 5), the ovaries were removed when a follicle in the final wave of the interovulatory interval reached the preovulatory stage. To ensure that the follicles collected for the preovulatory follicle collection were those destined to ovulate, only the ewes with one ovulatory-sized follicle (≥ 5 mm in diameter) during the estrus period were used. All ovaries were immediately snap-frozen after dissection and stored at −80°C. A total of forty-three follicles were collected from 19 ewes.

Immunohistochemistry and histology

A cryostat microtome (Leica CM3050 S; Leica Microsystems, Nußloch, Germany) was used to obtain 10-µm thick frozen sections from each follicle [7]. Terminal deoxynucleotidyl transferase-mediated dUTP-biotin nick end labeling (TUNEL *in situ* cell detection kit, POD; catalogue no. 1684717; Roche Molecular Biochemicals, Penzburg, Germany) was used to identify apoptotic cells in the granulosa layer. The follicles used in this study were all deemed "healthy", as the overall percentage of apoptotic cells in the granulosa ranged from 0 to 16.3% [7].

Immunohistochemistry was used to detect steroidogenic enzymes (CYP17, CYP19 and 3β-HSD). The primary antibodies were against 3β-HSD (rabbit polyclonal antibody against CYP17; mouse monoclonal antibody against human CYP17A1 provided

by Dr. CR Parker Jr, University of Alabama, Birmingham); CYP19 (mouse monoclonal antibody against human CYP19A1; catalogue no. MCA2077T; Cedarlane Laboratories, Hornby, ON, Canada) and recombinant human type II 3β-HSD (provided by Dr JI Mason, University of Edinburgh; validated for sheep gonads [17]). The negative controls were normal mouse IgG for CYP17 and CYP19, and normal rabbit serum for 3β-HSD. Immunoreactivity was detected with HRP-conjugated goat anti-mouse/rabbit immunoglobulins (Dako Diagnostics, Mississauga, ON, Canada) and a peroxidase substrate kit (Vector® VIP, Vector Laboratories, Burlingame, CA, USA). Staining intensities were quantified by gray-scale densitometric analysis of immunohistochemical slides as previously described [18]. Briefly, the mean gray-scale values were used to calculate the absorptive indices of immunohistochemical specimens. The mean gray-scale value through a clear glass slide with a coverslip was considered 100% transmittance, while the mean gray-scale value obtained by blocking the light path of the microscope was considered 0% transmittance. All mean gray-scale values obtained for follicles were then converted to the percentage transmittance. The values for percentage transmittance were averaged for the 4 samples per follicle and transformed to absorbance (negative value of the log of the percentage transmittance), and the absorptive index was calculated [19] by obtaining the ratio of absorbance of the reactive to nonreactive areas. This method of reporting the results has been demonstrated to provide considerable advantage over other semiquantitative methods because the absorptive index value is independent of the tissue section thickness [20]. Lastly, the specific absorptive index for each follicle was calculated by subtracting the absorptive index of a section treated with steroid enzyme-adsorbed primary antisera (nonspecific reactions) from the absorptive index of sections treated with non-adsorbed primary antisera.

Granulosa thickness was determined from histological slides at an image magnification of 100x. It was measured in pixels, using a line measuring tool, and then converted to S.I. units (μm).

Spot analysis of follicular antrum

Computerized image analyses were preceded by a second, more precise measurement of ovarian antral follicles taken from still ultrasonographic images. All follicles were then categorized as small (≥ 2.00 mm and ≤ 3.50 mm, n = 18), medium (> 3.50 mm and ≤ 4.50 mm, n = 9) or large (> 4.50 mm in diameter, n = 11) follicles of the first follicular wave of the interovulatory interval studied, or preovulatory antral follicles (n = 5). Echotextural analyses of follicular images were done using commercially available image analysis software (Image ProPlus®, Media Cybernetics, San Diego, CA, USA). Two individuals to whom identities of ovarian images and ewes were not known performed all analyses. The analysis of the follicular antrum was done by placing a circular computer-generated spot at the center of each follicle. The size of the spot was enlarged progressively until the follicular wall was encountered, as evidenced by an increase in numerical pixel values at the antrum-wall interface; the diameter of a spot meter was then decreased by approximately two pixels and the values were recorded. This technique was used to ensure that only the antrum was included in analysis of nonspherical follicles. The mean gray-scale value (mean value of all pixels within the measuring spot), pixel heterogeneity (standard deviation of numerical pixel values within the spot), and minimum and maximum pixel values were recorded.

Line analysis of ovarian follicles

Line analysis was used to measure the gray-scale pixel values along a straight, computer-generated line that was 3 pixels in length was placed over and encompassing the follicular wall [11]. The linear distance corresponding to one pixel was calculated by measuring the length of the 10-mm scale bar on the ultrasound images in pixels and was estimated to be 125 μm. A user-selected line was placed at approximately the 2 and 10 o'clock positions; these locations were selected to avoid the confounding effects of shadowing (refraction) artifacts. A two-dimensional graph was then computed for each line, which corresponded to the numerical values of each pixel along the length of the line. The interface of the antrum and follicular wall was identified by the first sharp increase in gray-scale values. Based on the results of a histomorphological study of ovine antral follicles, data for only a part of the line including one pixel (segment length) inward from the antrum-wall interface (peripheral antrum), one pixel outward from the interface (follicular wall proper) and one more pixel outward from the follicular wall (perifollicular ovarian stroma) were used for image analyses. The mean pixel intensity and pixel heterogeneity (standard deviation of numerical pixel values) were computed for each of the three line segments. The *y*-intercept (the point at which the line intercepts with the vertical axis) and slope (the angle from the horizontal line) for a line within each pixel segment were also calculated using the *x*, *y* coordinates for the points at the beginning and end of each pixel segment. There were no differences ($P > 0.05$) between the two lines or individuals performing the image analyses; therefore, the mean values for the echotextural variables of the antrum (central and peripheral), follicular wall proper and perifollicular stroma were calculated by taking the average of two (spot analysis) or four values (line analysis; 2 lines × 2 individuals).

Statistical analyses

One-way ANOVA (SigmaPlot® for Windows® version 11.0, 2008; Systat Software, Richmond CA, USA) was performed for the echotextural variables in each follicle category and for granulosa layer thickness, steroidogenic enzyme expression of the 3 enzymes and TUNEL results (% of positive granulosa cells). The Pearson's product-moment correlations (SigmaPlot®) were computed among follicular diameters and echotextural variables, granulosa layer thickness, steroidogenic enzyme expression (specific absorptive indices) and TUNEL results. When the normality test failed, a Kruskal-Wallis one-way ANOVA on ranks was used. All data are presented as least square means ± SEM. P values ≤ 0.05 were regarded as significant.

Acknowledgments

The present study was funded by the Natural Sciences and Engineering Research Council of Canada (NSERC) Discovery Grants to Drs NC Rawlings and PM Bartlewski, Alberta Agricultural Research Institute (NCR), and statutory funds of the Department of Swine and Small Ruminant Breeding at the University of Agriculture in Kraków, Poland. Thanks are extended to Drs LP Reynolds and AJ Conley for provision of antibodies for immuno-

histochemistry of steroidogenic enzymes; Drs K Janardhan, RJ Rodgers, B Singh, J Singh and Mr J Gibbons for their help with cryosectioning and immunohistochemistry of ovine ovarian sections; Mr I Shirley for his assistance with densitometric analyses; and Drs ET Bagu, DMW Barrett, K Davies and SV Seekallu for their help with ultrasonography and ovariectomies. Animal care was provided by the staff of the Animal Care Unit at the Western College of Veterinary Medicine, University of Saskatchewan.

References

1. **Rochira V, Carani C.** Aromatase deficiency in men: a clinical perspective. *Nat Rev Endocrinol* 2009; **5**: 559–568. [Medline] [CrossRef]
2. **Miyaura C, Toda K, Inada M, Ohshiba T, Matsumoto C, Okada T, Ito M, Shizuta Y, Ito A.** Sex- and age-related response to aromatase deficiency in bone. *Biochem Biophys Res Commun* 2001; **280**: 1062–1068. [Medline] [CrossRef]
3. **Magoffin DA.** Ovarian enzyme activities in women with polycystic ovary syndrome. *Fertil Steril* 2006; **86**(Suppl 1): S9–S11. [Medline] [CrossRef]
4. **Vassena R, Adams GP, Mapletoft RJ, Pierson RA, Singh J.** Ultrasound image characteristics of ovarian follicles in relation to oocyte competence and follicular status in cattle. *Anim Reprod Sci* 2003; **76**: 25–41. [Medline] [CrossRef]
5. **Conley AJ, Kaminski MA, Dubowsky SA, Jablonka-Shariff A, Redmer DA, Reynolds LP.** Immunohistochemical localization of 3 beta-hydroxysteroid dehydrogenase and P450 17 alpha-hydroxylase during follicular and luteal development in pigs, sheep, and cows. *Biol Reprod* 1995; **52**: 1081–1094. [Medline] [CrossRef]
6. **Huet C, Monget P, Pisselet C, Monniaux D.** Changes in extracellular matrix components and steroidogenic enzymes during growth and atresia of antral ovarian follicles in the sheep. *Biol Reprod* 1997; **56**: 1025–1034. [Medline] [CrossRef]
7. **Duggavathi R, Janardhan K, Singh J, Singh B, Barrett DMW, Davies KL, Bagu ET, Rawlings NC.** Patterns of expression of steroidogenic enzymes during the first wave of the ovine estrous cycle as compared to the preovulatory follicle. *Anim Reprod Sci* 2006; **91**: 345–352. [Medline] [CrossRef]
8. **Pierson RA, Adams GP.** Computer-assisted image analysis, diagnostic ultrasonography and ovulation induction: strange bedfellows. *Theriogenology* 1995; **43**: 105–112. [CrossRef]
9. **Liu X, Hart EJ, Petrik JJ, Nykamp SG, Bartlewski PM.** Relationships between ultrasonographic image attributes, histomorphology and proliferating cell nuclear antigen expression of bovine antral follicles and corpora lutea ex situ. *Reprod Domest Anim* 2008; **43**: 27–34. [Medline]
10. **Singh J, Pierson RA, Adams GP.** Ultrasound image attributes of bovine ovarian follicles and endocrine and functional correlates. *J Reprod Fertil* 1998; **112**: 19–29. [Medline] [CrossRef]
11. **Wu D, Barrett DMW, Rawlings NC, Giffin JL, Bartlewski PM.** Relationships of changes in ultrasonographic image attributes to ovulatory and steroidogenic capacity of large antral follicles in sheep. *Anim Reprod Sci* 2009; **116**: 73–84. [Medline] [CrossRef]
12. **Ahmadi B, Mirshahi A, Giffin J, Oliveira MEF, Gao L, Hahnel A, Bartlewski PM.** Preliminary assessment of the quantitative relationships between testicular tissue composition and ultrasonographic image attributes in the ram. *Vet J* 2013; **198**: 282–285. [Medline] [CrossRef]
13. **Bell JR, Mellor KM, Wollermann AC, Ip WT, Reichelt ME, Meachem SJ, Simpson ER, Delbridge LM.** Aromatase deficiency confers paradoxical postischemic cardioprotection. *Endocrinology* 2011; **152**: 4937–4947. [Medline] [CrossRef]
14. **Tom JW, Pierson RA, Adams GP.** Quantitative echotexture analysis of bovine ovarian follicles. *Theriogenology* 1998; **50**: 339–346. [Medline] [CrossRef]
15. **Wickenheisser JK, Nelson-DeGrave VL, Hendricks KL, Legro RS, Strauss JF 3rd, McAllister JM.** Retinoids and retinol differentially regulate steroid biosynthesis in ovarian theca cells isolated from normal cycling women and women with polycystic ovary syndrome. *J Clin Endocrinol Metab* 2005; **90**: 4858–4865. [Medline] [CrossRef]
16. **Thomas ST, Yang X, Sampson NS.** Inhibition of the M. tuberculosis 3β-hydroxysteroid dehydrogenase by azasteroids. *Bioorg Med Chem Lett* 2011; **21**: 2216–2219. [Medline] [CrossRef]
17. **Quirke LD, Juengel JL, Tisdall DJ, Lun S, Heath DA, McNatty KP.** Ontogeny of steroidogenesis in the fetal sheep gonad. *Biol Reprod* 2001; **65**: 216–228. [Medline] [CrossRef]
18. **Singh J, Adams GP.** Immunohistochemical distribution of follistatin in dominant and subordinate follicles and the corpus luteum of cattle. *Biol Reprod* 1998; **59**: 561–570. [Medline] [CrossRef]
19. **Fritz P, Multhaupt H, Hoenes J, Lutz D, Doerrer R, Schwarzmann P, Tuczek HV.** Quantitative histochemistry. Theoretical background and its application in biology and surgical pathology. *Prog Histochem Cytochem* 1992; **24**: 1–53. [Medline]
20. **Heitz PU.** Immunocytochemistry—theory and application. *Acta Histochem Suppl* 1982; **25**(Suppl): 17–35. (Jena). [Medline]